Journal of Engineering Mathematics **33:** 141–156, 1998.

Concerning closed-streamline flows with discontinuous boundary conditions

M. VYNNYCKY*
Tohoku National Industrial Research Institute, 4-2-1 Nigatake, Miyagino-Ku, Sendai 983, Japan

Received 3 December 1996; accepted in revised form 6 October 1997

Abstract. High-Reynolds-number (Re) flow containing closed streamlines (Prandtl-Batchelor flows), within a region enclosed by a smooth boundary at which the boundary conditions are discontinuous, is considered. In spite of the need for local analysis to account fully for flow at points of discontinuity, asymptotic analysis for Re $\ll 1$ indicates that the resulting mathematical problem for determining the uniform vorticity (ω_0) in these situations, requiring the solution of periodic boundary-layer equations, is in essence the same as that for a flow with continuous boundary data. Extensions are proposed to earlier work [3] to enable ω_0 to be computed numerically; these require coordinate transformations for the boundary-layer variables at singularities, as well as a two-zone numerical integration scheme. The ideas are demonstrated numerically for the classical circular sleeve.

Key words: Batchelor flow, circular sleeve, periodic boundary layer, two-zone integration scheme.

1. Introduction

It is now well-established that a steady, two-dimensional laminar high-Reynolds-number (Re) flow with closed streamlines, driven by the motion of the boundary surrounding it, will contain viscous boundary layers which enclose inviscid patches of constant vorticity [1]. A question of considerable interest in such situations is whether the value of the constant vorticity, ω_0, can be determined by asymptotic means for Re $\ll 1$, since its calculation ensures the mathematical closure of the flow under consideration.

Methods for evaluating the value of ω_0 have been derived already, although under certain restrictions. For flows on the interior of a smooth boundary, subject to continuous boundary conditions, Riley [2] and Vynnycky [3] have presented methods which both inevitably require the numerical integration of periodic boundary-layer equations, but which differ in the way they use the converged data. Riley's method exploits the fact that the solution has to be obtained numerically, with a finite computational domain being used to approximate a semi-infinite region, to derive a numerical matching condition for the shear stress at the outer boundary of the domain. Vynnycky's method, on the other hand, involves the derivation of an integral constraint from the area integral of the Navier-Stokes equations which contains $O(1)$ and $O(\mathrm{Re}^{-1/2})$ terms which can be determined after the $O(1)$ boundary-layer equations have been solved. Agreement between the methods is found to be very good for flows inside a family of ellipses with eccentricity as high as 0·77; in addition, actual Navier-Stokes computations carried out by Haddon and Riley [4], and extrapolated in the limit as Re $\to \infty$, indicate quantitative agreement with the asymptotic methods.

In addition to this approach, which seeks to solve the boundary-layer equations fully, an alternative route has been pursued by Lyne [5] and Chernyshenko [6] for dealing with flows

* Present address: Department of Mechanics, Royal Institute of Technology, S-100 44 Stockholm, Sweden.

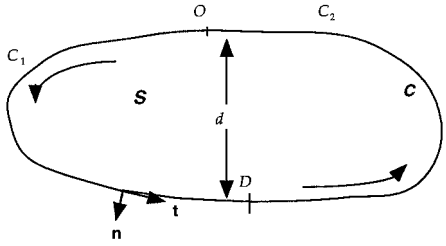

Figure 1. Geometry for closed-streamline flow.

within boundaries containing (i) discontinuous boundary conditions; (ii) corners or cusps; and (iii) mixing layers. These authors solve a linearised form of the boundary-layer equations in order to determine ω_0, and the method has subsequently been used by Chernyshenko [7, 8] and Chernyshenko and Castro [9, 10] in a variety of problems involving flow separation, thereby clarifying certain issues concerning the asymptotic structure of flow past a bluff body [11–13]. Nonetheless, the only *exact* treatment of periodic boundary-layer equations remains that due to Riley [2] and Vynnycky [3], and an important question to ask is whether their methods can be adapted to problems containing any of (i), (ii) or (iii), all the more so since Prandtl-Batchelor flows containing these difficulties continue to attract significant attention [14–19]. In this paper, the main focus of attention is (i).

Both [2] and [3] express reservations concerning the evaluation of ω_0 in flows when the driving boundary condition is discontinuous, however. Hitherto, the only regime where this has been possible has been for the circular sleeve considered by Batchelor [1], for which numerical computations were not even necessary. We formulate this class of problem in Section 2, and identify discontinuities in boundary conditions as being a generalization of those in classical external flow past a finite plate. In order to obtain the full flow details for that problem, local analysis is necessary in the vicinity of the leading and trailing edges of the plate; to be sure, an analogous procedure would be necessary for interior flows. By considering the circular sleeve as a test problem, it is demonstrated that these local details are not actually necessary for determining ω_0; all that is required is the analytical inclusion, by means of a two-zone calculation scheme, of the tiered flow-structure downstream of a discontinuity. An alternative, simpler, criterion to that used in [3] is derived and applied in order to determine ω_0.

2. Formulation

2.1. Equations

Consider a region S surrounded by a smooth closed curve C, as in Figure 1. The steady motion of C, across which it is assumed there is no normal outflow, induces a high-Re flow within S. Furthermore, the tangential motion of C is prescribed in terms of the streamwise velocity on a portion (C_1) of C and in terms of the shear stress on the remainder (C_2); the flow is assumed not to separate, and all streamlines are closed. The dimensionless governing flow equations in primitive-variable formulation are then

$$\nabla \cdot \mathbf{u} = 0, \qquad (\mathbf{u} \cdot \nabla)\mathbf{u} = -\nabla p + \delta^2 \nabla^2 \mathbf{u}. \tag{2.1a,b}$$

where $\mathbf{u}$ is the velocity vector, p is the pressure and $\delta (= \mathrm{Re}^{-1/2})$ is, as usual, the boundary-layer thickness; here, the Reynolds number is given by $\mathrm{Re} = \rho U d/\mu$, where ρ is the fluid

density, U is a typical velocity scale, d is a typical length scale for the region S and μ is the coefficient of viscosity.

As for the boundary conditions, the requirement for no normal outflow is given by

$$u_i n_i = 0 \quad \text{on } C, \tag{2.2}$$

and that for the tangential flow by

$$u_i t_i = U_c \quad \text{on } C_1, \tag{2.3a}$$

and

$$\frac{\partial u_i}{\partial n_i} = \tau_C \quad \text{on } C_2; \tag{2.3b}$$

here $(n_i)_{i=1,2}$ are the Cartesian components of the outward normal, **n** to C, $(t_i)_{i=1,2}$ are the components of the tangent, **t**, to C, $(u_i)_{i=1,2}$ the components of the velocity vector **u**, and U_C and τ_C are functions of the arc length of C which may have jump discontinuities on C_1 and C_2 respectively, and which denote the prescribed tangential velocity and shear stress, respectively.

Now, introduce the core stream function, vorticity, pressure and velocity component expansions as

$$\psi = \psi_0 + \delta\psi_1 + O(\delta^2), \qquad \omega = \omega_0 + \delta\omega_1 + O(\delta^2), \qquad p = p_0 + \delta p_1 + O(\delta^2),$$

$$u_i = u_{0i} + \delta u_{1i} + O(\delta^2), \quad i = 1, 2$$

and the asymptotic expansions for the boundary-layer streamfunction, tangential velocity and pressure (Ψ, U, P, respectively), as

$$\Psi = \Psi_0 + \delta\Psi_1 + O(\delta^2), \qquad U = U_0 + \delta U_1 + O(\delta^2), \qquad P = P_0 + \delta P_1 + O(\delta^2);$$

it is well-known from the Prandtl-Batchelor theorem that ω_0 is a constant, which is unknown *a priori*. For the boundary layer at C, we have at leading order (dropping the subscripts on Ψ_0)

$$\Psi_N \Psi_{Ns} - \Psi_s \Psi_{NN} = \omega_0^2 u_\infty \dot{u}_\infty + \Psi_{NNN}, \tag{2.4}$$

where $(\dot{})$ denotes differentiation with respect to the arc length s, and N is the boundary-layer coordinate along the inward normal to C, where $|\mathbf{n}| \sim \delta$, so that $N \sim O(1)$; here, the rescaled stream function, Ψ, is related to ψ by $\psi = \delta\Psi$. The boundary conditions for the boundary layer are

$$\Psi = 0 \quad \text{on } N = 0, \tag{2.5a}$$

$$\Psi_N \to \omega_0 u_\infty(s) \quad \text{as } N \to \infty, \tag{2.5b}$$

and the flow-driving condition given by

$$\Psi_N = U_C(s) \quad \text{on } N = 0, \qquad 0 \leqslant s \leqslant s_{C_1} \tag{2.5c}$$

and

$$\Psi_{NN} = \tau_C(s) \quad \text{on } N = 0, \qquad s_{C_1} < s \leqslant L, \tag{2.5d}$$

where L denotes the total length of the curve C and s_{C_1} denotes the length of C_1; in (2.5b), $u_\infty(s)$ is the canonical tangential velocity at C derived from $\hat{\psi} := \omega_0\psi$, so that

$$u_\infty(s) = \left(\frac{\partial\hat{\psi}}{\partial n_i}t_i\right)_C. \tag{2.6}$$

We also expect the periodicity requirement

$$\Psi(0, N) = \Psi(L, N), \quad \forall N \geqslant 0, \tag{2.7}$$

in addition to which a constraint on ω_0, as given either by Riley [2] or Vynnycky [3], determines ω_0 uniquely, thus closing the problem.

Without loss of generality, take a reference point, O, on C to be at one of the common points of C_1 and C_2, and consider any point on C at which the flow-driving boundary condition is discontinuous (call it D and denote by s_D the distance OD); D may either be one of the points C_1 or C_2, or one of the points within C_1 and C_2 at which U_C or τ_C, respectively, are discontinuous. The situation at D is a generalization of that at either the leading or trailing edge of a finite flat plate, as considered by Goldstein [20]. In the latter case, it is well-known that the attached flow strategy holds, with the Blasius' boundary layer upstream giving way to the Goldstein near-wake solution downstream, provided there is a triple-deck region of streamwise extent $O(\mathrm{Re}^{-3/8})$ in which the singularity that is induced in the pressure, as a result of the switch from a no-slip to a no-shear boundary condition, is accommodated. In the former case, which constitutes the start of the Blasius' boundary layer, the singularity at the leading edge is treated by means of a square region of extent $O(\mathrm{Re}^{-1}) \times O(\mathrm{Re}^{-1})$; with both singular points accounted for, subsequently, there is essentially no difficulty in treating the flow field hierarchically in terms of asymptotic expansions for the flow variables.

To incorporate these ideas into the present interior problem, we note first that, for the leading edge of the classical problem, $U_C(s_{D-}) = 1, U_C(s_{D+}) = 0$ whilst for the trailing edge, $U_C(s_{D-}) = 0, \tau_C(s_{D+}) = 0$. Thus, the classical problem contains two out of a host of possible combinations in which U_C and τ_C can be permuted upstream and downstream of s_D, each requiring individual analytical treatment. At first glance, we might conjecture that there are 14 possibilities, which arise from permuting

$$U_C(s_{D-}) \neq 0, \qquad U_C(s_{D-}) = 0, \qquad \tau_C(s_{D_-}) \neq 0, \qquad \tau_C(s_{D_-}) = 0$$

with their equivalents for s_{D+}, but subtracting the two cases where

$$U_C(s_{D-}) = U_C(s_{D+}) = 0, \qquad \tau_C(s_{D_-}) = \tau_C(s_{D_+}) = 0.$$

In reality, there are fewer cases to consider since the analysis for the case where $\tau_C(s_{D-})$ is prescribed will lead to the same treatment of the discontinuity as does the case for $U_C(s_{D-}) \neq 0$; however, as we shall see later, there is a significant difference between the cases

$$U_C(s_{D-}) \neq 0, \qquad U_C(s_{D+}) = 0, \quad \text{and } U_C(s_{D+}) \neq 0, \qquad U_C(s_{D-}) = 0.$$

We do not intend to examine the structures for all cases, but instead to verify these ideas for the only case in which an analytical solution is known: the circular sleeve. To keep the development as general as possible, we first formulate a generic sleeve-type problem, based on Batchelor's [1], in which a part of the boundary C is at rest, while the rest is taken to move with a general slip velocity U_s.

3. A generalized sleeve

Assume without loss of generality that the no-slip boundary lies between $s = s_1(:= 0)$ and $s = s_2$, so that

$$U_C(s) = \begin{cases} 0 & \text{if } s_1 \leqslant s \leqslant s_2, \\ U_s(s) & \text{if } s_2 \leqslant s \leqslant L; \end{cases} \tag{3.1}$$

here, U_s is taken to be a continuous function of s which is positive for $s_2 < s < L$, and is such that $U_s(s_1) > 0, U(s_2) > 0$. Also, for later use, define by $(R_j, \Theta_j)_{j=1,2}$ local plane polar coordinates which are centred on the points at $s = (s_j)_{j=1,2}$, respectively; in particular, define each Θ_j in such a way that $\Theta_j \to 0$ as $s \to s_{j_+}$, and $\Theta_j \to \pi$ as $s \to s_{j_-}$ so that for all points on and within $C, 0 \leqslant \Theta_j \leqslant \pi$.

3.1. The discontinuity at $s = s_1$

In order to accommodate the change in boundary condition at $s = s_1$, a two-tier flow structure is required downstream; in the lower tier, $N/(s - s_1)^{1/2} \sim O(1)$, whilst in the upper, $N \sim O(1)$. Introducing the substitutions

$$\Psi = (s - s_1)^{1/2} F(s, \eta), \qquad \eta = N \left(\frac{\lambda_1}{s - s_1} \right)^{1/2}, \tag{3.2}$$

where $\lambda_1 = \min(1, s_2 - s_1)$ (for reasons to be explained later), we observe that (2.4) becomes

$$\lambda_1^{1/2} F''' + \left(\frac{s - s_1}{\lambda_1} \right) \omega_0^2 u_\infty \dot{u}_\infty + \tfrac{1}{2} F F'' = (s - s_1) \left(F' \frac{\partial F'}{\partial s} - F'' \frac{\partial F}{\partial s} \right), \tag{3.3}$$

where $(')$ denotes differentiation with respect to η. Introducing further the expansion

$$F = F_0(\eta) + (s - s_1)^{1/2} F_1(\eta) + (s - s_1) F_2(\eta) + \cdots, \tag{3.4}$$

for the lower tier, and

$$\Psi = \Psi_0(N) + (s - s_1)^{1/2} \Psi_1(N) + (s - s_1) \Psi_2(N) + \cdots, \tag{3.5}$$

for the upper, we consider the limit as $s \to s_{1_+}$. For $(s - s_1)^0$, (3.3) reduces to

$$\lambda_1^{1/2} F_0''' + \tfrac{1}{2} F_0 F_0'' = 0, \tag{3.6}$$

subject to

$$F_0(0) = 0, \qquad F_0'(0) = 0, \qquad F_0'(\infty) = U_s(s_{1_-}) \lambda_1^{-1/2}, \tag{3.7a,b,c}$$

with the last equation coming from matching to the upper tier. For the purposes of verifying the numerical scheme, to be introduced later, it is also worth determining Ψ_1, as follows. Substituting (3.5) in (2.4), we equate the leading terms at $O(s-s_1)^{1/2}$ to obtain

$$\Psi_{0N}\Psi_{1N} - \Psi_{0NN}\Psi_1 = 0, \tag{3.8}$$

which gives

$$\Psi_1(N) = \mathcal{A}_1\Psi_{0N}, \tag{3.9}$$

where $\mathcal{A}_1$ is a constant which comes from matching the upper and lower tiers at $(s-s_1)^{1/2}$; more specifically,

$$\mathcal{A}_1 = \frac{C_0^{(1)}}{U_s(s_{1-})}, \tag{3.10}$$

where

$$C_0^{(1)} = \lambda_1^{-1/2}\int_0^\infty (U_s(s_{1-}) - \lambda_1^{1/2}F_0')\,\mathrm{d}\eta, \tag{3.11}$$

these two equations being valid even if the boundary for $s = s_{1+}$ were not at rest. The fact that it is at rest, however, ensures a canonical solution $\hat{F}_0(\hat{\eta})$, where

$$\hat{F}_0 = U_s(s_{1-})^{-1/2}F_0, \qquad \hat{\eta} = \left(\frac{U_s(s_{1-})}{\lambda_1}\right)^{1/2}\eta;$$

for the present case then,

$$C_0^{(1)} = 1{\cdot}7208(U_s(s_{1-}))^{1/2}, \tag{3.12}$$

whence

$$\mathcal{A}_1 = 1{\cdot}7208(U_s(s_{1-}))^{-1/2}. \tag{3.13}$$

Note here that the introduction of λ_1 was optional, but its inclusion proves useful for the numerical scheme and later generalizations. Furthermore, F_1 is given by the solution to

$$\lambda_1^{1/2}F_1''' + \tfrac{1}{2}(F_0F_1'' - F_0'F_1') + F_1F_0'' = 0, \tag{3.14}$$

subject to

$$F_1(0) = 0, \qquad F_1'(0) = 0, \qquad F_1 \sim \tfrac{1}{2}\Psi_{0NN}(0)\eta^2, \quad \text{as } \eta\to\infty. \tag{3.15a,b,c}$$

Equations for the higher terms in both expansions can be derived in similar fashion.

The situation is now similar to that for the leading edge of a Blasius plate, except that the incoming velocity profile is not uniform. Nonetheless, the change in boundary conditions still induces fractional algebraic behaviour in ψ_1, even though ψ_1 in this case is not irrotational; the required details are determined as follows. The function ψ_1 can be decomposed into

an irrotational part, $\hat{\psi}_1$, which satisfies boundary conditions that are induced by the $O(1)$ boundary-layer flow, that is

$$\hat{\psi}_1 = -\int_0^\infty (\Psi_N(s,\infty) - \Psi_N(s,N))\,\mathrm{d}N \quad \text{on } C, \tag{3.16}$$

and a rotational part, ψ_1^*, which has constant vorticity, ω_1, and satisfies homogeneous boundary conditions (see [3] and Appendix A). ψ_1^* is simply a constant multiple of ψ_0 and therefore exhibits no singular behaviour at C, so the focus of attention is $\hat{\psi}_1$. Using (3.9)–(3.16), we arrive at

$$\hat{\psi}_1 \sim -\int_0^\infty (\Psi_N(s_1,\infty) - \Psi_N(s_1,N))\,\mathrm{d}N + A_1(s-s_1)^{1/2}, \tag{3.17}$$

for the behaviour of $\hat{\psi}_1$ as $s \to s_{1_+}$, where $A_1 = \mathcal{A}_1\Psi_{0N}(\infty)$.

Near $R_1 = 0$,

$$\hat{\psi}_1 + \int_0^\infty (\Psi_{0N}(\infty) - \Psi_{0N}(N))\,\mathrm{d}N \sim A_1 R_1^{1/2}\cos\frac{\Theta_1}{2}, \tag{3.18}$$

from which it follows that, since p_1 is given by

$$p_1 = -(u_{0i}u_{1i} + \omega_0\psi_1 + \omega_1\psi_0), \tag{3.19}$$

we have

$$p_1 \sim -\tfrac{1}{2}\mathcal{A}_1[\Psi_{0N}(\infty)]^2(s-s_1)^{-1/2}. \tag{3.20}$$

In this case, the induced pressure force becomes comparable with the leading order inertial forces ($\Psi_N\Psi_{Ns} \sim (s-s_1)^{-1}$) when

$$s - s_1 = O(\mathrm{Re}^{-1}). \tag{3.21}$$

Thus, a square $O(\mathrm{Re}^{-1}) \times O(\mathrm{Re}^{-1})$ region, in which the full Navier-Stokes equations hold, is required around the discontinuity; such a problem has been solved numerically by Van de Vooren and Djikstra [21]. We comment further on this region's significance in Section 3.3.

3.2. The discontinuity at $s = s_2$

At $s = s_2$, the transition from a no-slip to slip boundary condition also requires a transformation to similarity variables in the form given by (3.2), except with λ_1 and s_1 replaced by $\lambda_2 = \min(1, L - s_2)$ and s_2 respectively, so that for $(s-s_2)^0$ we arrive at

$$\lambda_2^{1/2}F_0''' + \tfrac{1}{2}F_0F_0'' = 0, \tag{3.22}$$

subject to

$$F_0(0) = 0, \qquad F_0'(0) = U_s(s_{2+})\lambda_2^{-1/2}, \qquad F_0'(\infty) = 0. \tag{3.23a,b,c}$$

It is now evident that expansions in $(s-s_2)^{1/2}$ of the form given by (3.4) and (3.5) cannot be valid, because lower and upper tier terms at $(s-s_2)^{1/2}$ could not then match; more precisely, F_0 has the property that

$$F_0 \sim C_0^{(2)} = 1{\cdot}6128(U_C(s_{2_+}))^{1/2} \quad \text{as } \eta \to \infty, \tag{3.24}$$

where

$$C_0^{(2)} = \lambda_2^{-1/2} \int_0^\infty (\lambda_2^{1/2} F_0' - U_s(s_{2_+}))\,\mathrm{d}\eta, \tag{3.25}$$

whereas (3.9) vanishes as $N \to 0$. Instead, the appropriate expansions are

$$F = F_0(\eta) + (s-s_2)^{1/4} F_1(\eta) + (s-s_2)^{1/2} F_2(\eta) + \cdots, \tag{3.26}$$

for the lower tier, and

$$\Psi = \Psi_0(N) + (s-s_2)^{1/4} \Psi_1(N) + (s-s_2)^{1/2} \Psi_2(N) + \cdots, \tag{3.27}$$

for the upper. Substitution of (3.27) in (2.4) again gives (3.8) and (3.9), although this time at $O(s-s_2)^{-3/4}$. At $O(s-s_2)^{-1/2}$, we obtain

$$\Psi_{0N}\Psi_{2N} - \Psi_2 \Psi_{0NN} = \tfrac{1}{2}(\Psi_1 \Psi_{1NN} - \Psi_{1N}^2), \tag{3.28}$$

which can be solved for Ψ_2 to give

$$\Psi_2 = \mathcal{A}_2 \Psi_{0N} + \tfrac{1}{2}\mathcal{A}_1^2 \Psi_{0NN}, \tag{3.29}$$

where $\mathcal{A}_2$ is a constant that could be determined by matching higher order terms in the asymptotic expansions; matching upper and lower tiers at $(s-s_2)^{1/2}$ gives

$$\mathcal{A}_1 = \left(\frac{2C_0^{(2)}}{\Psi_{0NN}(0)} \right)^{1/2}. \tag{3.30}$$

This provides the constant necessary to find F_1 which is given by the solution of

$$\lambda_1^{1/2} F_1''' + \tfrac{1}{4}(2F_0 F_1'' - F_0' F_1') + \tfrac{3}{4} F_1 F_0'' = 0, \tag{3.31}$$

subject to

$$F_1(0) = 0, \qquad F_1'(0) = 0, \qquad F_1 \sim \mathcal{A}_1 \eta, \quad \text{as } \eta \to \infty. \tag{3.32a,b,c}$$

For the behaviour of $\hat{\psi}_1$ as $s \to s_{2_+}$, we have

$$\hat{\psi}_1 \sim -\int_0^\infty (\Psi_{0N}(\infty) - \Psi_{0N}(N))\,\mathrm{d}N + A_2(s-s_2)^{1/4}, \tag{3.33}$$

where $A_2 = \mathcal{A}_1 \Psi_{0N}(\infty)$ and near $R_2 = 0$,

$$\hat{\psi}_1 + \int_0^\infty (\Psi_{0N}(\infty) - \Psi_{0N}(N))\,\mathrm{d}N \sim A_2 R_2^{1/4} \cos \tfrac{1}{4}\Theta_2; \tag{3.34}$$

thence

$$p_1 \sim -\tfrac{1}{4}\mathcal{A}_1[\Psi_{0N}(\infty)]^2(s-s_2)^{-3/4}, \tag{3.35}$$

so that the induced pressure and inertia forces become comparable when

$$\mathrm{Re}^{-1/2}(s-s_2)^{-7/4} \sim (s-s_2)^{-1}, \tag{3.36}$$

i.e.

$$s - s_2 \sim \mathrm{Re}^{-2/3}. \tag{3.37}$$

This suggests that the details of a square region of extent $O(\mathrm{Re}^{-2/3}) \times O(\mathrm{Re}^{-2/3})$ will have to be considered for a full description of the flow, although this proves to be unnecessary for the purposes of this paper.

3.3. Discussion

Since the length scales of the square regions at both discontinuities are much smaller than that of the boundary-layer thickness, it seems plausible to assume that the starting velocity profile for the flow downstream of the discontinuity should simply be taken as the incoming velocity profile just upstream; the situation is then the same as that which occurs when discontinuities are not present. In this sense, there is no actual need to solve the problems outlined in Sections 3.1 and 3.2 for the $O(\mathrm{Re}^{-1}) \times O(\mathrm{Re}^{-1})$ and $O(\mathrm{Re}^{-2/3}) \times O(\mathrm{Re}^{-2/3})$ regions, respectively. As regards the method of [2], no further preliminaries are required prior to proceeding to a numerical solution from which ω_0 may be determined. As a simpler alternative to [3], however, the following is proposed.

We note first, using [2], that the behaviour of Ψ as $N \to \infty$ may be written as

$$\Psi \sim N\omega_0 u_\infty(s) + f(s) + o(1),$$

where f is given by

$$f(s) = -\int_0^\infty (\omega_0 u_\infty(s) - \Psi_N)\,\mathrm{d}N.$$

Then, taking the first integral with respect to N of (2.4) over $[0,\infty)$ and rearranging, we obtain

$$\frac{\partial}{\partial s}\left[\int_0^\infty (\Psi_N^2 - \omega_0^2 u_\infty^2(s))\,\mathrm{d}N\right] - \omega_0 u_\infty(s)\dot{f}(s) = -\Psi_{NN}(0,s), \tag{3.38}$$

whence taking the integral around C gives

$$\oint_C (\Psi_{NN}(0,s) + \omega_0 \dot{u}_\infty(s) f(s))\,\mathrm{d}s = 0, \tag{3.39}$$

since the first term of the left-hand side of (3.38) vanishes, while the second may be integrated by parts. Consequently, ω_0 can be determined from the solution of the viscous boundary-layer equations at leading order alone, without recourse to the flow field at $O(\delta)$.

4. Numerical method

The numerical task at hand then is to solve (2.4) subject to the boundary conditions (2.5a), (2.5b) and (3.1), and the periodicity requirement (2.7), although the presence of discontinuities in boundary conditions requires modifications to the boundary-layer solvers used previously by Riley [2] and Vynnycky [3]; here, we propose to extend the latter. From Section 3, it is evident that flow downstream of each discontinuity will be two-tiered in nature; the numerical treatment of such flows is not unknown (for example, Smith [22], Veldman [23], Cebeci *et al.* [24]). In those problems, a 'working' solution can still be obtained for no-slip to no-shear boundary-condition changes by simply marching with the same independent variables as were used upstream of the discontinuity, in the sense that judicious mesh refinement downstream of the discontinuity may still give acceptable results; however, a two-zone scheme to take account of the discontinuity is unavoidable for the sleeve problem, because of the square-root singularity in the shear stress, as shown in Section 3.1 and 3.2.

As in [3], a Keller-Box discretisation [25, pp. 213–234] was used to discretise the governing equations, which were expressed in differing variables depending on the value of s at C. For $s_1 \leqslant s \leqslant s_1 + \lambda_1$, (3.3) was discretised for the lower tier, whilst (2.4) was used for the upper; for $s_2 \leqslant s \leqslant s_2 + \lambda_2$, (2.4) was again used for the upper, whilst (3.3), with the appropriate replacements for λ_2 and s_2, was used for the lower. On all remaining portions of C, (2.4) only was used, the introduction of λ_1 and λ_2 now being apparent, since the fact that $\eta \equiv N$ at $s = s_1 + \lambda_1$ and $s = s_2 + \lambda_2$ ensures a tidy transition from two-zone to physical variables. The manner in which, in the two-zone region, the upper and lower tiers are matched has been discussed in detail before [24], so we omit the majority of the details here; the only difference arises because the similarity variables used are different, so that the numerical matching conditions here are, for $j = 1, 2$,

$$\Psi\left(s, \eta_\infty \left(\frac{s - s_j}{\lambda_j}\right)^{1/2}\right) = (s - s_j)^{1/2} F(s, \eta_\infty), \tag{4.1a}$$

$$\Psi_N\left(s, \eta_\infty \left(\frac{s - s_j}{\lambda_j}\right)^{1/2}\right) = \lambda_j^{1/2} F_\eta(s, \eta_\infty), \tag{4.1b}$$

$$\Psi_{NN}\left(s, \eta_\infty \left(\frac{s - s_j}{\lambda_j}\right)^{1/2}\right) = \frac{\lambda_j}{(s - s_j)^{1/2}} F_{\eta\eta}(s, \eta_\infty), \tag{4.1c}$$

where η_∞ denotes the position of the interface between the upper and lower regions, which is given in the physical (s, N)-plane by

$$N = \eta_\infty \left(\frac{s - s_j}{\lambda_j}\right)^{1/2}.$$

Throughout, uniform spacing was used for the N-direction, as well as for s-values lying in the one-zone calculation region; for each of the two-zone regions ($j = 1, 2$), uniform spacing in $(s - s_j)^{1/2}$ was used.

For an arbitrary value of ω_0, the integration procedure was started at $s = s_1$ by prescribing some initial profile for Ψ, such as

$$\Psi = U_s(s_{1-})N + (\omega_0 u_\infty(s_1) - U_s(s_{1-}))(N + \mathrm{e}^{-N} - 1), \tag{4.2}$$

in the upper tier, and F_0, given by the solution to (3.6) and (3.7a)–(3.7c), for F in the lower; once $s = s_2$ has been reached, F_0 given by (3.22) and (3.23a)–(3.23c) is used to start up the lower tier. The integration was continued until the periodicity condition (2.7) had been satisfied to within a given tolerance; for most runs, 10^{-6} was used.

To iterate for ω_0, Brent's method, as given in [26, pp. 251–254], was used as a faster alternative to the bisection method used in [3]; once the root for ω_0 has been bracketed, only three or four iterations are required to satisfy (3.39) to within a tolerance of 10^{-7}. Lastly comes the question of evaluating the integrals in (3.39). The asymptotic behaviour for $\Psi_{NN}(0, s)$ at each of the points of discontinuity is given, from Sections 3.1 and 3.2, by

$$\Psi_{NN}(s, 0) \sim \frac{0{\cdot}33206(U_s(s_{1-}))^{\frac{3}{2}}}{(s - s_1)^{1/2}}, \quad \text{as } s \to s_1+, \tag{4.3a}$$

$$\Psi_{NN}(s, 0) \sim -\frac{0{\cdot}44385(U_s(s_{2+}))^{\frac{3}{2}}}{(s - s_2)^{1/2}}, \quad \text{as } s \to s_2+. \tag{4.3b}$$

These can be subtracted off from $\Psi_{NN}(0, s)$, and their contribution to (3.39) evaluated analytically. The remaining integrand is then finite-valued and can be evaluated using, for example, the alternative extended Simpson's rule [26, pp. 108].

5. Solution for the circular sleeve

When C is taken to be a circular boundary, it is known [1] that the core vorticity is given by

$$\int_0^{2\pi} U_C^2(s)\,\mathrm{d}s = \omega_0^2 \int_0^{2\pi} u_\infty^2(s)\,\mathrm{d}s; \tag{5.1}$$

in particular, if part of the boundary is at rest and the remainder moves with constant tangential velocity $\omega_C/2$, then

$$\omega_0 = \omega_C(1 - \sigma)^{1/2}, \tag{5.2}$$

where $0 < \sigma < 1$ is the proportion of the boundary that is at rest. Our intention, therefore, is to work towards the result of Equation (5.2) using the preceding ideas, which can then be applied for non-circular boundaries where (5.1) no longer holds, as well for more general discontinuous driving boundary conditions.

For a circle, the core streamfunction at $O(1)$ is just

$$\psi_0 = \tfrac{1}{2}\omega_0(1 - r^2), \tag{5.3}$$

so that $u_\infty(s) = \frac{1}{2}$. Furthermore, since $\dot{u}_\infty(s) \equiv 0$, (3.39) reduces in this case to just

$$\oint_C \Psi_{NN}(0, s)\,\mathrm{d}s = 0. \tag{5.4}$$

We set $s_2 = 2\pi\sigma, L = 2\pi$ and $U_s(s) \equiv \omega_C/2$, and consider in particular a sleeve of unit length, so that $\sigma = 1/2\pi$, with

$$\omega_C = \frac{2}{\left(1 - \frac{1}{2\pi}\right)^{1/2}}; \tag{5.5}$$

thus, we expect $\omega_0 = 2$. The location of the outer edge of the boundary layer, N_∞, was set to 20, this value having already been found in earlier work [2, 3] to be more than adequate to take account of the e^{-N} decay in the tangential velocity; computations were carried out using two mesh spacings (ΔN) for the N-direction, $\Delta N = \frac{1}{50}, \frac{1}{25}$, with Richardson extrapolation in ΔN then being used to determine ω_0 more accurately. For the two-zone regions, these were also the mesh spacings used for $\delta\eta$, the outer edge of the lower zone (η_∞) being taken at $\eta_\infty = 10$. This value needs to be sufficiently large to give the correct asymptotic behaviour as $\eta \to \infty$ for the starting similarity solutions just downstream of each boundary-condition discontinuity. This, in turn, may be assessed by monotoring the quantities $\hat{F}_0''(0)$ and $\hat{C}_0^{(j)}$ for $j = 1, 2$, where

$$\hat{C}_0^{(1)} = C_0^{(1)}/U_s(s_{1-}), \qquad \hat{C}_0^{(2)} = C_0^{(2)}/U_s(s_{2+});$$

in particular, with $\eta_\infty = 10, \Delta N = \frac{1}{25}$, we find for $j = 1$,

$$\hat{F}_0''(0) = 0{\cdot}33205, \qquad \hat{C}_0^{(1)} = 1{\cdot}7209$$

compared with the theoretical values 0·33206 and 1·7208 respectively, whilst for $j = 2$

$$\hat{F}_0''(0) = -0{\cdot}44384, \qquad \hat{C}_0^{(2)} = 1{\cdot}6128$$

compared with the theoretical values $-0{\cdot}44385$ and 1·6128 respectively.

Furthermore, for the ΔN-values given above, the integration in the two-zone region begins with around 750 and 1500 points respectively, with one point being dropped from the upper zone at each step in s. Taking the order of 10^2 points in s for s-stations in the one-zone region, we have the order of 10^3 points for the whole of C. Setting a tolerance of 10^{-5} in the Newton iteration at each step for $(\Psi, \Psi_N, \Psi_{NN})$ across the boundary layer, around 30 seconds of CPU time on a Cray Supercomputer was required to integrate around C once for $\Delta N = \frac{1}{50}$; on average, around 50 loops were required to satisfy the periodicity criterion to within a tolerance of 10^{-6}, giving a total of around 1300 CPU seconds for one value of ω_0. The total time required, once Brent iteration had been implemented, was of the order of 5000 CPU seconds, with far fewer loops being required for a new value of ω_0, since integration could be started with the most-recently computed Ψ-profile, rather than (4.2).

The results of computations, as well as an extrapolation, are compared with the theoretical value in Table 1. Agreement is found to be good, although one reminder is necessary concerning the h^2-extrapolation. This had been carried out for the mesh spacing in N only (and not in both N and s as in [2, 3]), since a mesh which is non-uniform in s has to be used. Thus, we should not expect an $O(h^2)$ error behaviour with respect to the theoretical value, although presumably computations with more s-stations should yield results whose extrapolation (in ΔN) should approach the theoretical value even more closely; however, we do not pursue this any further here.

Table 1. Comparison of analytical and computed values for ω_0.

	ω_0
$\Delta N = \frac{1}{25}$	2·0021
$\Delta N = \frac{1}{50}$	2·0011
extrapolated	2·0008
theoretical	2·0

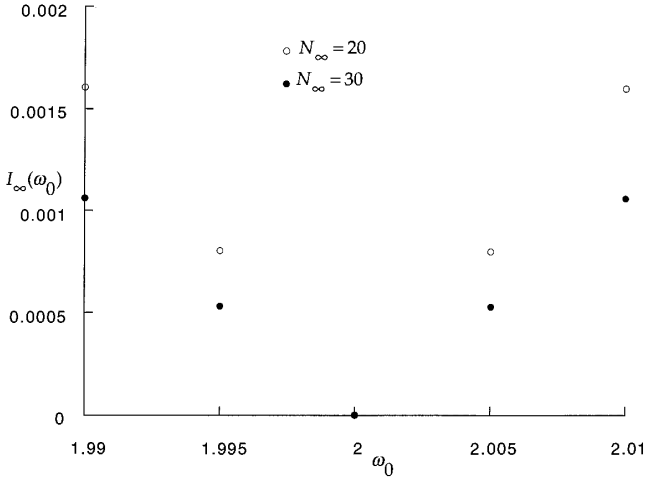

Figure 2. I_∞ as a function of ω_0 for $N_\infty = 20, 30 (\Delta N = \frac{1}{50}, \frac{3}{100}$, respectively).

Additional runs were carried out for $N_\infty = 30$ with 1001 points in the N-direction, primarily to verify the dependence of I_∞, defined

$$I_\infty(\omega_0) := \oint_C \left| \frac{\partial^2 \Psi}{\partial N^2} \right|_{N=N_\infty} \mathrm{d}s, \tag{5.6}$$

on N_∞; this behaviour, in the vicinity of $\omega_0 = 2$, is given in Figure 2. As one would expect (*cf.* [2]), I_∞ is found to decrease with increasing N_∞. Clearly evident here is the presence of a minimum close to $\omega_0 = 2$ which constitutes the required root; for this value of ω_0, I_∞ is of the order of 10^{-6} for both values of N_∞, so that the two points overlap on the diagram. A more systematic approach to determine ω_0 more accurately would involve using Brent's method, for example, to solve

$$\frac{\mathrm{d}I_\infty}{\mathrm{d}\omega_0} = 0, \tag{5.7}$$

although this was not done here in the interests of minimising computational expense. Note here, incidentally, the relation between the two criteria, (5.4) and (5.7). In considering the numerical implementation of (5.4), one might argue that because a finite computational domain is being used, the correct condition should be

$$\oint_C \Psi_{NN}(0, s)\, \mathrm{d}s = \oint_C \Psi_{NN}(N_\infty, s)\, \mathrm{d}s; \tag{5.8}$$

Table 2. Comparison of analytical and numerical values of constants in Equation (5.8) for $\omega_0 = 2{\cdot}0011 (N_\infty = 20, \Delta N = \frac{1}{50})$.

	numerical	analytical
α_1	0·5001	0·5
A_1	−1·6500	−1·6487
α_2	0·2481	0·25
A_2	3·0726	2·8307

thus, one would expect the constraints (5.7) and (5.4) to agree on the root for ω_0.

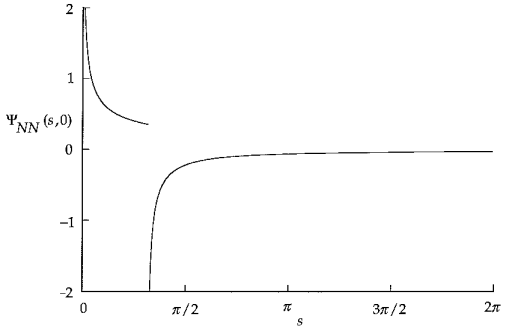

Figure 3. Ψ_{NN} at $N = 0$ *vs.* s for $\omega_0 = 2{\cdot}0010 (N_\infty = 20, \Delta N = \frac{1}{50})$.

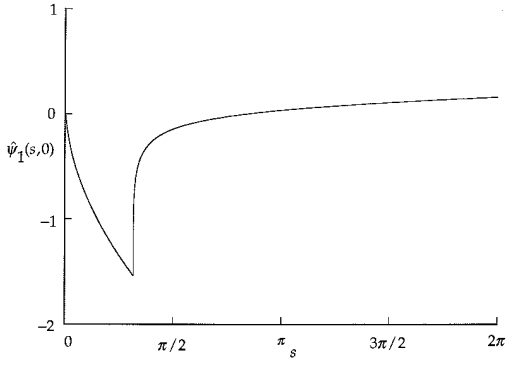

Figure 4. ψ_1 at C *vs.* s for $\omega_0 = 2{\cdot}0010 (N_\infty = 20, \Delta N = \frac{1}{50})$.

Figures 3 and 4 show, respectively, the shear stress Ψ_{NN} and $\hat{\psi}_1$ at $N = 0$ for $\Delta N = \frac{1}{50}$ with $\omega_0 = 2{\cdot}0011$. In the first case, the square root singularities in Ψ_{NN} downstream of the discontinuities are evident; in the second, we see that $\hat{\psi}_1$ has a discontinuous gradient at these points. The local behaviour of Ψ_{NN} at $N = 0$ has been incorporated into the numerical method already thanks to the coordinate transformation, although that of $\hat{\psi}_1$, given by Equations (3.17) and (3.33), serves as a useful check that the two-zone scheme is working correctly. Taking the computed values of $\hat{\psi}_1(0, s)$ at $s = (s_j)_{j=1,2}$ and the next two mesh points downstream, and assuming the behaviour of $\hat{\psi}_1(s, 0)$ to be of the form

$$\hat{\psi}_1(s, 0) \sim \hat{\psi}_1(s_j, 0) + A_j (s - s_j)^{\alpha_j}, \quad j = 1, 2, \tag{5.9}$$

we obtain the real constants $(\alpha_j, A_j)_{j=1,2}$ and compare these with analytical values found in Sections 3.1 and 3.2; this is done in Table 2. Agreement for the α_j values is found to be good. For A_j, the theoretical values of which are

$$A_1 = 0{\cdot}8605 \omega_0 \left(1 - \frac{1}{2\pi}\right)^{1/4}, \tag{5.10a}$$

$$A_2 = \tfrac{1}{2}\omega_0 \left(\frac{3{\cdot}232}{\Psi_{0NN}(0)}\right)^{1/2} \left(1 - \frac{1}{2\pi}\right)^{1/8}, \tag{5.10b}$$

agreement is within the order of 2% for $j = 1$, but not so good for $j = 2$; note, however, that for A_2, even the so-called theoretical value relies on the numerical computation of $\Psi_{0NN}(0)$, which only becomes available once the boundary-layer integration has reached s_2. A possible explanation for the differing levels of agreement in the two cases may lie in the fact that the next term in the expansion for $\hat{\psi}_1(s, 0)$ at $s = s_1$ is $O(s - s_1)$, whereas at $s = s_2$ it is $O(s - s_2)^{1/2}$. Consequently, there is a greater likelihood that an estimate for the constant of proportionality based on $\hat{\psi}_1(s, 0)$-values at three points will be less accurate for s_2 than for s_1; viewed a different way, the two downstream points that are taken for s_2 should be taken much closer to s_2 than is the case for s_1, in order for the correct asymptotic behaviour to become apparent from the numerical data.

6. Conclusion

This paper has considered closed-streamline flows which are driven by discontinuous boundary conditions. The introduction of such discontinuities introduces both analytical and numerical complications which are not present in flows where the boundary conditions are continuous. Analytically, discontinuities induce a pressure gradient on the boundary layer which exceeds that due to the Euler pressure at distances sufficiently close to the discontinuity itself; in this case, the situation is similar to that encountered in external flow past a finite plate. When obtaining a numerical solution, we note that it is necessary to take account of the two-tier boundary-layer structure that appears downstream of a discontinuity by introducing a coordinate transformation for the lower tier. These ideas have been applied to the circular sleeve problem, which is the only case for which analytical comparison appears to be available; however, provided the boundary layer remains attached, there seems nothing to prevent the application of these ideas to closed-streamline flows with more general smooth boundaries and more general discontinuous boundary conditions.

Finally, it is worth noting that interesting and challenging extensions of this work involve its potential applicability to boundaries with corners or cusps [5, 27], as well as to flows containing an inviscid patch of constant vorticity and a region of inviscid potential flow [28], or flows containing more than one patch of constant vorticity [18]. With reference to the last two, it is to be expected that boundary-layer computations should help to select the value of ω_0, and hence the Euler solution, that constitutes the limiting solution of the Navier-Stokes equations as Re $\to \infty$.

Appendix A

To show that ω is constant to all orders of δ, it is known that for the core flow $\omega = \omega(\psi)$, so that the line integral of (2.1b), taken around C, in the limit as $\delta \to 0$, gives

$$\frac{\mathrm{d}\omega}{\mathrm{d}\psi} \oint_C \mathbf{q}{\cdot}\mathbf{t}\, \mathrm{d}s = 0, \tag{A.1}$$

whence, since this implies that $\mathrm{d}\omega/\,\mathrm{d}\psi = 0, \omega$ is constant. In addition, if we write $\omega = \omega_0 + \omega^*$, where ω^* denotes lower order terms in the asymptotic expansion of ω, such that $|\omega^*| \ll |\omega_0|$, with ω_0 as the leading order term, we have that $\omega^* = \omega^*(\psi)$, and thence (A.1) applies to ω^* also, so that ω^* too is constant. Hence ω is constant to all orders, as required.

Acknowledgements

The author wishes to acknowledge the financial support of the European Union, and helpful discussions with Andrew Fowler.

References

1. G. K. Batchelor, On steady laminar flow with closed streamlines at large Reynolds number. *J. Fluid Mech.* 1 (1956) 177–190.
2. N. Riley, High Reynolds number flows with closed streamlines. *J. Eng. Math.* 15 (1981) 15–27.
3. M. Vynnycky, On the uniform vorticity in a high Reynolds number flow. *J. Eng. Math.* 28 (1994) 129–144.
4. E. W. Haddon and N. Riley, On flows with closed streamlines. *J. Eng. Math.* 19 (1985) 233–246.
5. W. H. Lyne, Unsteady viscous flow in a curved pipe. *J. Fluid Mech.* 45 (1970) 13–31.
6. S. I. Chernyshenko, An approximate method of determining the vorticity in the separation region as the viscosity tends to zero. *Fluid Dyn.* 17 (1982) 1–11.
7. S. I. Chernyshenko, The calculation of separated flows of low viscosity liquids using the Batchelor model. *Library translation 2133, RAE* (1985).
8. S. I. Chernyshenko, The asymptotic form of the steady separated flow past a body at large Reynolds number. *Appl. Math. Mech.* 52 (1988) 746–753.
9. S. I. Chernyshenko and I. P. Castro, High Reynolds-number asymptotics of the steady flow through a row of bluff bodies. *J. Fluid Mech.* 257 (1996) 421–449.
10. S. I. Chernyshenko and I. P. Castro, High Reynolds-number weakly stratified flow past an obstacle. *J. Fluid Mech.* 317 (1996) 155–178.
11. F. T. Smith, A structure for laminar flow pasta bluff body at high Reynolds number. *J. Fluid Mech.* 155 (1985) 175–191.
12. D. H. Peregrine, A note on the steady high Reynolds-number flow about a circular cylinder. *J. Fluid Mech.* 157 (1985) 493–500.
13. F. T. Smith, Concerning inviscid solutions for large-scale separated flows. *J. Eng. Math.* 20 (1986) 271–292.
14. R. McLachlan, A steady separated viscous corner flow, *J. Fluid Mech.* 231 (1991) 1–34.
15. G. Giannakidis, Prandtl-Batchelor flow in a channel. *Phys. Fluids A* 5 (1993) 863–867.
16. C. Turfus, Prandtl-Batchelor flow past a flat plate at normal incidence in a channel – inviscid analysis. *J. Fluid Mech.* 249 (1993) 59–72.
17. G. Giannakidis, Prandtl-Batchelor flow on a circular cylinder and on aerofoil sections. *Aeronaut. J.* 100 (1996) 15–26.
18. M. Vynnycky and K. Kanev, Coupled Batchelor flows in a confined cavity. *J. Fluid Mech.* 319 (1996) 305–322.
19. A. V. Bunyakin, S. I. Chernyshenko and G.Y. Stepanov, Inviscid Batchelor-model flow past an airfoil with a vortex trapped in a cavity. *J. Fluid Mech.* 323 (1996) 367–376.
20. S. Goldstein, Concerning some solutions of the boundary-layer equations in hydrodynamics. *Proc. Camb. Phil. Soc.* 26 (1930) 1–30.
21. A. J. Van de Vooren and D. Djikstra, The Navier-Stokes solution for laminar flow past a semi-infinite plate. *J. Eng. Math.* 4 (1970) 9–27.
22. F. T. Smith, Boundary-layer flow near a discontinuity in wall conditions. *J. Inst. Maths and its Applics.* 13 (1974) 127–145.
23. A. E. P. Veldman, A new calculation of the wake of a plate. *J. Eng. Math.* 9 (1975) 65–70.
24. T. Cebeci, F. Thiele, P. G. Williams and K. Stewartson, On the calculation of symmetric wakes I. Two-dimensional flows. *Num. Heat Transf.* 2 (1979) 35–60.
25. T. Cebeci and P. Bradshaw, *Momentum Transfer in Boundary Layers*. Washington: Hemisphere Publishing Corporation (1977) 391pp.
26. W. H. Press, B. P. Flannery, S. A. Teukolsky and W. T. Vetterling, *Numerical Recipes: The Art of Scientific Computing*. Cambridge: Cambridge University Press (1989) 818pp.
27. E. W. Haddon and N. Riley, A note on the mean circulation in standing waves. *Wave Motion* 5 (1983) 43–48.
28. D. W. Moore, P. G. Saffman and S. Tanveer, The calculation of some Batchelor flows: The Sadovskii vortex and rotational corner flow. *Phys. Fluids* 31 (1988) 978–990.